ELSEVIER

Order in the disordered state: local structural entities in the fast ion conductor $Ba_2In_2O_5$

Chris E. Mohn[a], Neil L. Allan[b], Colin L. Freeman[b], P. Ravindran[a], Svein Stølen[a],*

[a]Department of Chemistry and Center for Materials Science and Nanotechnology, University of Oslo, Post Box 1033 Blindern, N0315 Oslo, Norway
[b]University of Bristol, School of Chemistry, Cantock's Close, Bristol BS8 1TS, England

Abstract

The structural features of $Ba_2In_2O_5$ at high temperatures are discussed based on a thorough study of the full energy hypersurface of a 36 atoms supercell by periodic density functional theory. The results obtained for this cell are furthermore used for considering stacking-sequences and connectivity-patterns present only in larger supercells. The distribution of oxygen vacancies is far from random and relatively few configurations, associated with different arrangements of tetrahedral InO_4, square pyramidal InO_5 and octahedral InO_6 entities, are thermally accessible at most temperatures. Our results call into the question of commonly used defect models for such grossly disordered materials in which oxygen vacancies are distributed at random over a number of lattice sites. The energetic preference for certain structural entities also has important implications for ionic transport due to restraints imposed by local symmetry.

© 2004 Elsevier Inc. All rights reserved.

Keywords: $Ba_2In_2O_5$; Local structure; Disorder; Ionic conduction

1. Introduction

While materials at low temperatures are often characterized in terms of crystal chemical concepts, descriptions of their high-temperature properties are usually based on defect chemistry. Both approaches are obviously of great value but also have clear limitations. While the defect chemistry is often weakly linked to the crystal structure of the material and basically provides an ideal solution model where the solutes are either simple defects or defect clusters, crystal chemistry most often gives a static view of the material and tries to reduce the real complex structure to one in which the local structure does not vary throughout the crystal. Thus descriptions based on partial occupancy and random distributions of different species are frequently encountered. In the present study we approach the local and average structure of a grossly disordered oxide, $Ba_2In_2O_5$, by configurational averaging using energies of individual configurations optimized by density functional theory. Our description bridges the two usual approaches for describing the structure of disordered materials and provides a unified picture of the main structural features of this excellent fast oxide ion conductor at both low and high temperatures.

$Ba_2In_2O_5$ adopts the brownmillerite-type structure which consists of alternating two-dimensional layers of corner-shared InO_4-tetrahedra and corner-shared InO_6-octahedra. When the structure was first determined, the InO_4 tetrahedra were assumed to be regularly ordered [1] with empty oxygen-sites, vacancies, arranged in parallel chains as shown in Fig. 1a. For clarity, the Ba-cations are not shown in the figure. There are three crystallographically distinct oxygen sites; O(1) in the equatorial plane of the octahedra, O(2) at the apical sites of the octahedra and O(3) those oxygens in the tetrahedra not shared with the octahedra. On heating

*Corresponding author. Fax: +47 2285 5441.
E-mail address: svein.stolen@kjemi.uio.no (S. Stølen).
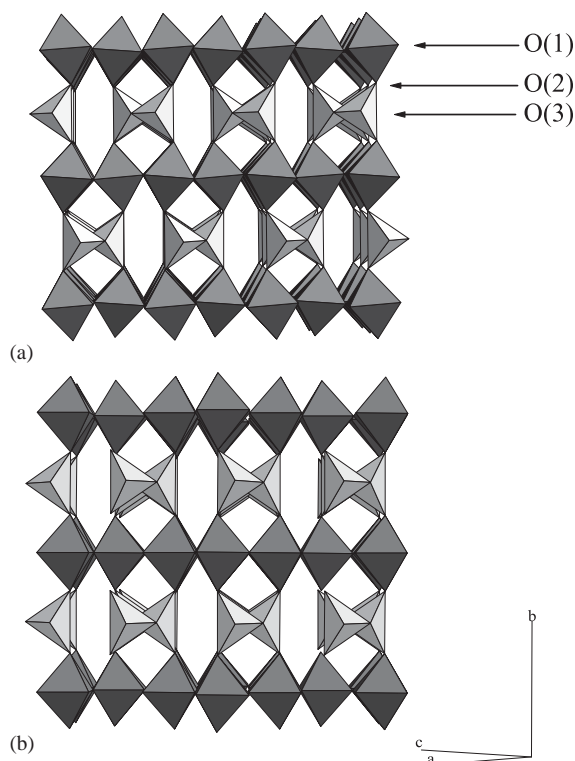
Fig. 1. Polyhedral-representation of the two lowest-energy brownmillerite-related CNCs. The three different oxygen sites are marked. The two CNCs differ in *stacking* of the tetrahedral layer; (a) the experimentally observed stacking where the vacancy channels are staggered along the *b*-axis; (b) the higher energy CNC where the vacancy channels are not staggered.

brownmillerite-type oxides, the entropy gain connected with disordering of oxygen atoms and vacancies often gives rise to order–disorder transitions. While the ionic conductivity is typically rather low in the vacancy-ordered modification, high oxygen-ion conductivities are often observed in the high-temperature modification. Our model system, $Ba_2In_2O_5$, shows a discontinuous jump in the ionic conductivity of more than one order of magnitude at 1203 K [2]. Above this temperature the oxide ion conductivity is equal in magnitude to that of the widely used stabilized zirconias. The structural aspects of the disordering are of considerable interest for understanding the ionic conductivity of this and related materials.

While the room temperature structure of $Ba_2In_2O_5$ was initially described as an ideal brownmillerite-type structure, space group *Ibm2* [1], two recent in situ neutron diffraction studies [3,4] indicate some degree of disorder to be present already at room temperature in that the InO_4 tetrahedra centered at the 8*i* position of space group *Icmm* may take two different orientations. The orientation of a given tetrahedron is unlikely to be random and the presence of domains in which all tetrahedra take just one of the two orientations has been suggested [3].

The structural features of the temperature-induced disordering are less clear. A two-step process in which the cubic high-temperature modification is formed via a tetragonal modification was suggested on the basis of NMR and X-ray diffraction data [5]. In the first step at 1200 K, these data suggest that the structure undergoes reorganization within the oxygen-deficient layers only. Above this temperature oxygen is transported two-dimensionally within the tetrahedral layers involving only O(3)-atoms through fluctuations involving long waves of cooperative tilt inversion. The number of mobile oxygen ions in the structure was observed to increase continuously on further heating up to 1350 K. Only above this temperature are all oxygens considered to be involved in the disorder and mobile [5]. However, even here the local structure still possesses some degree of order; but only over a length scale too small to be observed by X-ray diffraction. The cubic structure in this picture possesses short-length-scale non-cubic microdomains [5]. Similar behavior has been proposed for other systems as well, e.g. Sr_2MnGaO_5 [6] and $Ba_3In_2ZrO_8$ [7]. In the latter case microdomains on length scales of 50–500 Å are observed.

The results of the two previously mentioned in situ neutron diffraction studies [3,4] do not preclude the proposed two-step disordering. Both neutron studies describe the cubic high-temperature structure as an oxygen deficient perovskite-type oxide $ABO_{3-\delta}$ with oxygen atoms and vacancies randomly distributed over a single oxygen site (occupancy 5/6). While Speakman et al. support the existence of two different structural transitions [4], Berastegui et al. suggest a single orthorhombic to cubic transition [3]. Even so, two-dimensional ion-conductivity at intermediate temperatures is not excluded by Berastegui et al. [3], but rather interpreted as due to a dynamic reorientation involving the two possible orientations of the InO_4-tetrahedra proposed for the low-temperature structure.

The only simulation study, a classical molecular dynamics simulation, reported for the disordered phase supports a two-stage transition [8]. The low-temperature orthorhombic structure transforms to a tetragonal structure that subsequently becomes cubic. In the tetragonal structure diffusion is suggested to be restricted to the sites around the tetrahedrally coordinated In-atoms. However, in contrast to the conclusions drawn from the NMR data by Adler et al. [5], both the O(2) and O(3) sites are involved in the ion movements. Oxygen-ions at the O(2) sites are suggested to be always the first to migrate while oxygen atoms at the O(1) sites are observed to migrate only at high temperatures. The latter is in agreement with the earlier discussed NMR/XRD-study [5].

In this paper the structural features of $Ba_2In_2O_5$ at high temperatures are investigated through a thorough study of the full energy hypersurface of a 36 atoms

supercell. The average structure observed experimentally is interpreted as a time and spatial average of the local structures corresponding to the different energetically accessible local energy minima of this cell. The results for this relatively small cell are furthermore used for considering stacking-sequences and connectivity-patterns present only in larger supercells. A preliminary account of the consequences of our model for the mechanism of the ionic conductivity has been published elsewhere [9].

2. Computational details

We investigate the structural features of $Ba_2In_2O_5$ through studying the energy hypersurface of a $2 \times 2 \times 2$ cell containing 36 atoms constructed by doubling a primitive cubic unit cell along each of the crystallographic directions. Initially 20 oxygen atoms are distributed over the 24 oxygen lattice sites of the ABO_3 supercell (giving 10626 *initial unrelaxed* arrangements). A symmetry routine reduces this total to 78 *initial unrelaxed* crystallographically non-equivalent arrangements. Structural optimizations with respect to *all* unit cell dimensions and atomic coordinates of each arrangement are performed using density functional theory within the generalized gradient approximation (GGA). No symmetry constraints were imposed during the optimizations. A sufficiently large basis of projected augmented plane waves (using a 222 *k*-mesh) was used as implemented in the Vienna ab initio simulation program (VASP) [10,11]. The optimizations are accompanied by large structural changes and thus an energy cut-off of 700 eV was needed for convergence. Inspection of the optimized configurations guides our approach for finding additional local energy minima. At this stage all O(3) sites of $Ba_2In_2O_5$ in the *Icmm* description are considered in addition to those of the ABO_3 lattice. A final total of 81 *relaxed* crystallographic non-equivalent configurations (CNCs) are thus obtained which, using the symmetry routine to determine the degeneracy of each CNC, gives a total of 21,500 *relaxed* local energy minima configurations. We stress the importance of full structural optimizations of each configuration. These are crucial since large energy changes (typically of the order of 1 eV per formula units) accompany the structural relaxations and these determine not only the magnitude of the energy differences between the CNCs but even the relative order of energies which changes after relaxation.

We use configurational (Boltzmann) averaging to calculate the fraction of the different polyhedra and the occupancy of the crystallographically distinct oxygen sites as a function of temperature (see for instance Refs. [12,13]). Given the Gibbs energy, G_k, for the *relaxed* (optimized) configurations k we then average

$$Y = \frac{\sum_{k=1}^{K} Y_k \exp(-G_k/k_B T)}{\sum_{k=1}^{K} \exp(-G_k/k_B T)}, \tag{1}$$

where K is the total number of local minima found on the potential energy hypersurface (21,500 minima), and Y is the structural property in question or the enthalpy, H. The entropy is given by

$$S = \frac{H}{T} + k_B \ln\left(\sum_{k=1}^{K} \exp(-G_k/k_B T)\right). \tag{2}$$

In this paper we ignore vibrational contributions to the Gibbs energy G_k of each configuration; the vibrational entropy and the vibrational contribution to the enthalpy is neglected and the energy of each configuration is generated in the static limit ($G_k = H_k^{\text{static}}$). Entropies calculated using the resulting values thus represents solely the *configurational* contribution to the total entropy of the system. Calculation of the vibrational entropy of all configurations would be computationally very expensive and we are thus not pursuing the vibrational entropy contribution to the total energetics here. Although some minor changes in relative energy might occur the overall description of the order in the disordered state would not be changed. An earlier study considers the effect of the vibrational entropy albeit in a simpler system [14].

3. Results and discussion

3.1. The energy spectrum and structural features of selected CNCs

The final energy vs. degeneracy plot for the $2 \times 2 \times 2$ cell is given in Fig. 2, where each symbol refers to a separate relaxed crystallographic non-equivalent configuration. Some configurations overlap in energy. The number given in brackets for some CNCs represents the number of indium atoms with 2, 3, 4, 5 and 6 oxygen nearest-neighbours, e.g. (00404) denotes configurations with four four-coordinate In-atoms and four six-coordinate In-atoms in the $2 \times 2 \times 2$ cell. The symbols in the figure give additional information as shown in the figure caption. Our choice of supercell does not permit the formation of the stacking of tetrahedral layers observed experimentally in the ordered low temperature form (see Fig. 1a). The energy of this structure is calculated from an orthorhombic 18-atom cell, defined as zero and shown by an open star in Fig. 2. Furthermore, the 36 atoms cell used in the simulations only contains four vacancies and thus configurations with less than 2 oxygen atoms around a given indium atom are not represented. Such configurations are expected to be high in energy.
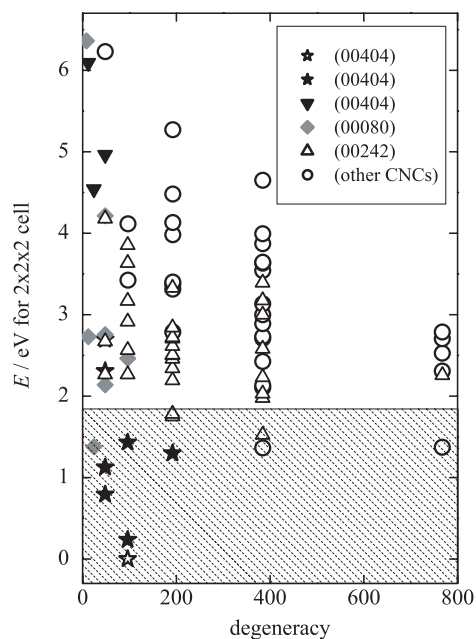
Fig. 2. Energy-degeneracy plot for a $2 \times 2 \times 2$ cell of $Ba_2In_2O_5$. Numbers in brackets show number of In-atoms with 2, 3, 4, 5 or 6 surrounding oxygen atoms (the total number of In-atoms is 8). The (00404) CNCs represented by filled stars contain InO_4-tetrahedra while those represented by triangles contain InO_4 square-planar entities. The energy of the experimentally observed structure is calculated from an orthorhombic 18-atom cell, defined as zero and shown by an open star. The dashed area identifies the energy region populated significantly at 2500 K (see text).

We interpret the average structure observed experimentally at any temperature as a time and spatial average of the different local environments (corresponding to separate local minima on the potential energy surface) which are energetically accessible at that temperature. These environments are regarded as representing snapshots of small regions of the disordered material and thus showing local structural environments and structural correlations. The structural features of some selected configurations and thus of the disordered phase will now be considered in some detail. The average structural and thermodynamic properties are considered later.

There are relatively few CNCs thermally accessible at most temperatures. The two lowest-energy CNCs are both (00404) and contain 50% octahedra and 50% tetrahedra. They resemble the brownmillerite-type structure in that their structures consist of alternating layers of InO_4-tetrahedra and InO_6-octahedra. They differ in the *stacking* of the tetrahedral layers. In the lowest energy CNC the experimentally observed stacking (see Fig. 1a) along the *b*-axis is present. The vacancy channels are staggered along this axis consistent with a reduction of the electrostatic interactions between the tetrahedral layers. The stacking sequence in the second of the two-lower energy CNCs is shown in Fig. 1b. Here

the vacancy channels are not staggered. Although the former stacking sequence of the tetrahedral layers is observed in most $A_2B_2O_5$ oxides with 50% tetrahedra and 50% octahedra the latter has been reported in one case; for $LaSrCuAlO_5$ in which however the intervening octahedra are severely Jahn–Teller deformed and better described as square pyramids [15].

Observed and calculated unit cell dimensions for the ground state structure are compared in Table 1 that also compares selected interatomic distances. The agreement is good.

In addition to brownmillerite-like configurations with different stacking sequences of the tetrahedral layer, configurations with different types of *connectivity* within the tetrahedral layers are obtained. Six different connectivity patterns are given in Fig. 3 in order of increasing energy (a)–(f). These represent the eight different (00404) CNCs with tetrahedral In obtained for our $2 \times 2 \times 2$ supercell. Fig. 3a shows the connectivity observed experimentally and also obtained theoretically for the two lowest-energy-CNCs (see Fig. 2). With increasing energy, CNCs characterized by edge-sharing tetrahedra (Fig. 3b), by zig-zag patterns of tetrahedra (Fig. 3c and d), by a four-ring pattern (Fig. 3e), and by stretched tetrahedra chains (Fig. 3f) are observed. It is obvious that the energies of the different connectivity patterns are largely influenced by the large Ba atoms and thus by the Ba–O interactions. These interactions are easily characterized using bond valence sums which correlate well with the stability of the different CNCs. The bond valence sum [16] falls into four groups; while the bond valence sum of the lowest energy CNCs are 1.81, it is 1.85 for the edge-sharing CNC, decreasing to about 1.73 for the zig-zag CNCs and finally to below 1.70 (1.69 and 1.66) for the two higher energy CNCs. It is clear that the Ba–O interactions are important for the energetics of the different connectivity patterns and thus for the CNCs.

The kinked low-energy chain-CNC of Fig. 3a is identical to that observed experimentally in a large number of brownmillerite-related compounds. Both L (left-hand) and R (right-hand) chains, which are two members of the same CNC, along the modulation direction [100] have been reported [6,17]. Among the connectivity patterns observed in the higher energy CNCs, we have been able to find only one in related oxide systems in the literature. Surprisingly this is the ring pattern seen in Fig. 3e. This connectivity-scheme is high in energy for $Ba_2In_2O_5$, even though it has recently been observed in two oxygen-rich relatives, $Sr_{2.2}Y_{0.8}Mn_2GaO_{7.9}$ [18] and $Sr_{0.7}Y_{0.3}CoO_{2.62}$ [19], where much higher bond valence sums suggests that this structure is favorable in these cases. Although the bonding in silicates is very different, it is worth noting that unbranched tetrahedral single chains of SiO_4 tetrahedra show a large variation in the degree of chain

Table 1
Experimental and calculated unit-cell dimensions, and selected interatomic distances of the ground state orthorhombic structure

a (Å)	b (Å)	c (Å)	References
6.0991(1)	16.7365(3)	5.9622(1)	Berastegui et al. [3]
6.0867(3)	16.7841(7)	5.9696(3)	Speakman et al. [4]
6.2790	16.8410	6.0848	Present calculation
		Speakman et al. [4] (using their *Ibm2* description)	Present calculation
In (octa)	In(octa)–O(1)	2.127×2	2.188×2
	In(octa)–O(1)	2.143×2	2.196×2
	In(octa)–O(2)	2.311×2	2.341×2
In (tetr)	In(tetr)–O(2)	2.012×2	2.096×2
	In(tetr)–O(3)	2.091×1	2.137×1
	In(tetr)–O(3)	2.109×1	2.144×1
Ba	Ba–O	2.607×1	2.667×1
	Ba–O	2.721×1	2.702×1
	Ba–O	2.770×1	2.805×1
	Ba–O	2.802×1	2.833×1
	Ba–O	2.852×1	2.878×1
	Ba–O	2.883×1	2.889×1
	Ba–O	2.959×1	2.900×1
	Ba–O	3.089×1	3.293×1
	Ba–O	3.432×1	3.666×1
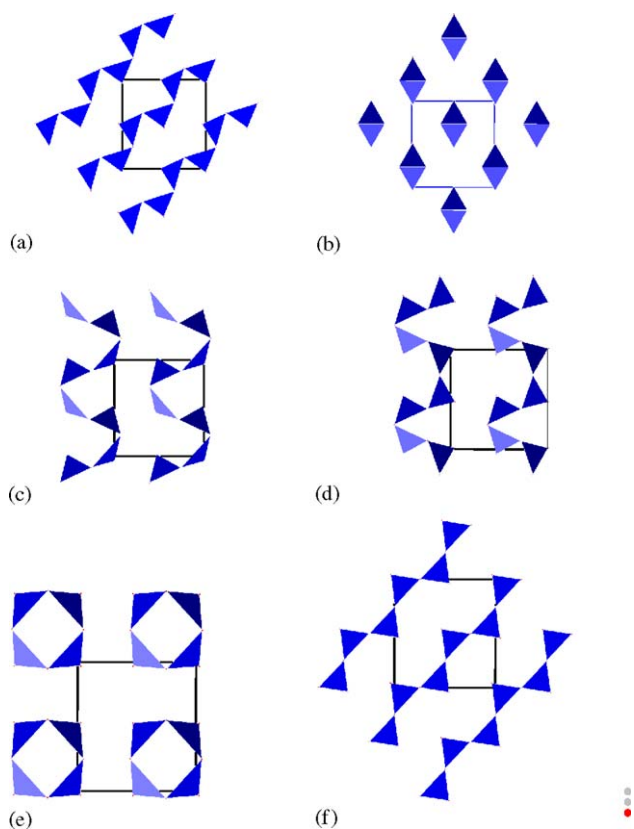
Fig. 3. Connectivity in the *ac*-plane of the different (00404) CNCs containing InO$_4$-tetrahedra in order of increasing (less negative) energy (a)–(f).

stretching in silicates and thus that patterns similar to the zig-zag patterns in Fig. 3c and d have been reported [20].

An interesting CNC close in energy to the (00404)-CNCs is one in which one oxygen vacancy is removed from each InO$_6$-octahedra yielding a structure built up from corner-sharing square pyramids. This (00080) structure resembles the ordered structure adopted by related compounds containing a Jahn–Teller ion such as Sr$_2$Mn$_2$O$_5$ [21] and Ca$_2$Mn$_2$O$_5$ (srebrodolskite) [22]. In addition, what may seem surprising at first sight is that also the structures of the high-energy configurations are quite simple. The highest and lowest energy (00080)-CNCs both contain rather regular polyhedra. While, the interatomic In–O distances for square pyramids in the lowest-energy (00080)-CNC are 2×2.14, 2×2.18 and 1×2.11 Å, four of the In–O distances are equal (4×2.15 Å) in the square pyramids of the highest-energy (00080)-CNC. The fifth In–O distance here is considerably shorter, 2.01 Å giving a "compressed" square pyramid. Again a clear correlation between the energetics and Ba bond valence sums is observed indicating that the positions of the large Ba-atoms play a key-role in determining the energies of the possible connectivities. This correlation is shown in Fig. 4 in which we plot the energies versus the Ba bond valence sums for the (00404) CNCs containing tetrahedral layers and the (00080) CNCs. The lowest energy (00080)-CNC is denser than the ground state implying that the former CNC containing only square pyramids is stabilized by pressure. The transformation of Sr$_2$Fe$_2$O$_5$, iso-structural with Ba$_2$In$_2$O$_5$, to a structure isostructural with Sr$_2$Mn$_2$O$_5$ below 15 GPa at ambient temperature shows that such a transformation may occur in brownmillerite-type oxides [23]. Also in the case of the (00080) CNCs some higher energy CNCs are stable in other systems;
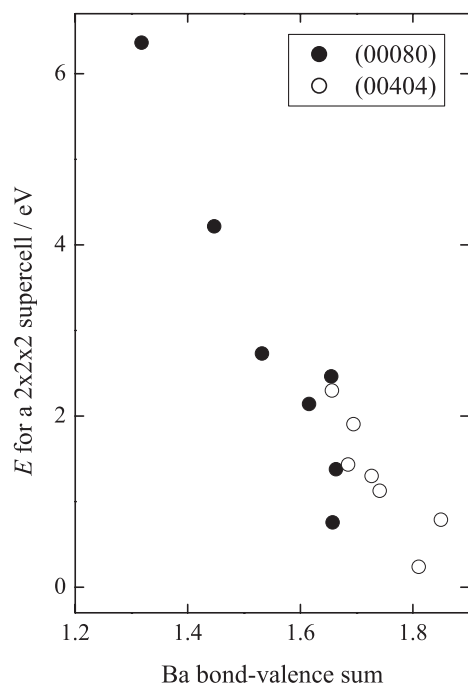
Fig. 4. Energy versus Ba bond valence sum for the (00404) CNCs containing tetrahedral layers and the (00080) CNCs.

the (00080) CNC at 2.73 eV is observed experimentally in $YBaFe_2O_5$ [24], $YBaMn_2O_5$ [25], and $YBaCo_2O_5$ [26], while that at 2.14 eV is similar to the structure suggested for $Ca_2Co_2O_5$ [27,28].

The high-energy (00404)s, marked with the black inverse triangles in Fig. 2, also contain 50% four coordinated and 50% six-coordinated indium. When two vacancies are introduced these may be located either on opposite sides or on the same face of the InO_6 octahedron and in this high-energy CNC the former prevails giving rise to square planar structural entities. The square planar geometry for In is in $Ba_2In_2O_5$, much less favorable than tetrahedral, in keeping with the molecular chemistry of indium. Square planar geometry is on the other hand frequently observed for late transition elements. $La_2Ni_2O_5$ containing Ni(II) (d^8) takes a crystal structure based on stacking of NiO_6-octahedra and NiO_4-square planar entities [29], which is essentially that of the highest-energy (00404) CNC.

Although the above discussion has covered significant features of the energy spectrum, it is important to remember that there are also more complex CNCs containing mixtures of octahedra, square pyramids and tetrahedra. It is however much more difficult to provide descriptive rationalizations of their relative stability. Although these more complex CNCs are high in energy for $Ba_2In_2O_5$, structures containing three different structural entities have been reported. One example is $La_{6.4}Sr_{1.6}Cu_8O_{20}$ for which the structure consists of rows of CuO_6 octahedra and CuO_5 square pyramids

running along the c-axis of the hexagonal structure, interconnected with CuO_4 square planar groups [30].

Other types of stacking sequences of the tetrahedral layers and connectivity patterns within the tetrahedral layers of (00404) CNCs will be present in larger supercells. Examples of such stacking sequences are sketched in Fig. 5. These different stacking sequences would be expected to be close in energy with small differences due to the relaxation that necessarily must accompany the changes in stacking. This suggests the incommensurate structure of Sr_2CuGaO_5 observed by high-resolution transmission electron microscopy [31] may be due to frozen-in disorder. While the energy difference between the different stacking sequences is low, the energy barriers for changing from one sequence to another must be thermally inaccessible at low temperatures and so complete long-range order is not easily achieved.

The vacancy channels in the two low-energy (00404) CNCs appear due to the presence of quasi-one-dimensional chains of corner sharing tetrahedra in the a,c-plane. In symmetrically equivalent configurations these chains have different orientations in the a,c-plane and hence an additional possibility in larger supercells is that the orientation of the chains in different tetrahedral layers is different. Such changes in orientation give rise to strain in the octahedral layers and test calculations on $2 \times 2 \times 4$ super cells show that such CNCs are high in energy.

Furthermore, the connectivity patterns in Fig. 3 intuitively suggest the existence of other types of connectivity-schemes for larger supercells. All these, with, e.g., different zig-zag patterns, larger ring systems would be higher in energy than the two lowest energy CNCs and our overall picture of the disordered material is essentially unchanged. In conclusion, a range of different configurations close in energy exists. Applying similar arguments to related compounds, the existence of different CNCs close in energy rationalizes the frequent observation of incompletely ordered structures even at room-temperature, e.g., for Sr_2MnGaO_5 [6], $Ca_2Co_{2-x}Al_xO_5$ [17], Sr_2CuGaO_5 [31], and LaBaCuGaO_5 [32].

3.2. Local structural entities and disorder

Disorder is a difficult topic to approach both experimentally and theoretically. Analyses of Bragg diffraction intensities give time-averaged structures but it is not possible to differentiate between disorder through reorientation of the polyhedra and static disorder due to the presence of domains. As we have mentioned Adler et al. [5] suggested from their NMR study that the two-dimensional conduction at intermediate temperatures in the monoclinic structure is due to long waves of cooperative octahedral tilt inversion
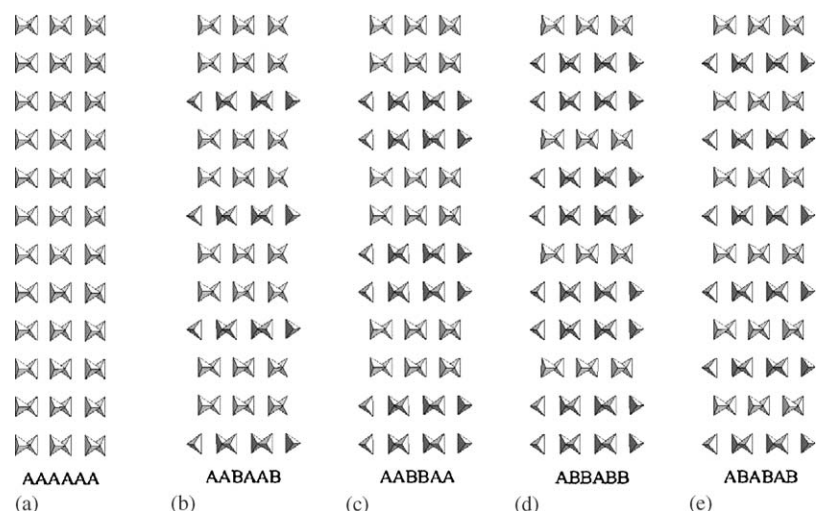
Fig. 5. Schematic representation of different possible stacking sequences along the *b*-axis of (00404) CNCs containing tetrahedral layers. The two lowest CNCs for the 36 atom cell are those denoted AAAAAA (a) and ABABAB (e); (b)–(d) are possible sequences requiring larger supercells. Those in between are hypothetical sequences. Only the tetrahedral layers are shown for clarity.

that travel through the crystal, allowing vacancy displacement within the tetrahedral layers. The preservation of monoclinic symmetry seen by X-ray diffraction is rationalized by Adler et al. [5] in terms of long-scale structural fluctuations larger than the length scale detected by X-ray diffraction (30 nm). The vacancies are thus considered ordered in a time-averaged sense [5]. Neutron diffraction data show the existence of an intermediate temperature tetragonal structure in which both the O(2) and O(3) ions exhibit large apparent temperature factors twice that of O(1) and comparable to those seen for the cubic high-temperature structure [4]. This may further support the cooperative tilting hypothesis. On increasing the temperature further $Ba_2In_2O_5$ becomes cubic. It is not clear whether this is due to dynamic or static disorder or both. Adler et al. [5] argue that the vacancies even at these temperatures may be ordered but over a length scale too small to be observed by X-ray diffraction and hence that the cubic structure has short-length-scale non-cubic microdomains. A similar hypothesis has been put forward for $Ba_3In_2ZrO_8$ where neutron diffraction shows that the material possesses long-range cubic symmetry but that randomly oriented local domains of 50–500 Å in size occur due to short-range ordering of the vacancies [7].

The fractions of the different polyhedra as a function of temperature, obtained by configurational averaging using the energy spectrum of Fig. 2, are plotted in Fig. 6. The magnitude of the temperature scale is affected by the size of the supercell, but nevertheless, this does not change our interpretation of the local order in the disordered state.

The high-energy configurations contribute only to a very limited degree even at high temperatures. The dashed area of Fig. 2 shows the energy region that
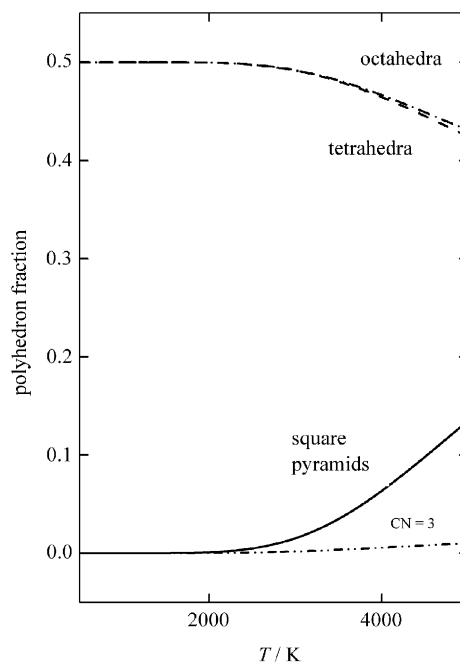
Fig. 6. Fraction of polyhedra as a function of temperature.

contributes significantly to the enthalpy at 2500 K; all other crystallographic non-equivalent configurations contribute less than 0.1%. The disordered system can thus be described in terms of populations of different local structural configurations all containing octahedra, square pyramids and tetrahedra. The fractions of octahedra and tetrahedra both remain close to 0.5 up to 1500 K. Although the (00404)-CNCs thus dominate at low temperatures disorder is not negligible. The range of different (00404)-configurations close in energy (see Fig. 2) gives rise to significant disorder and implies that
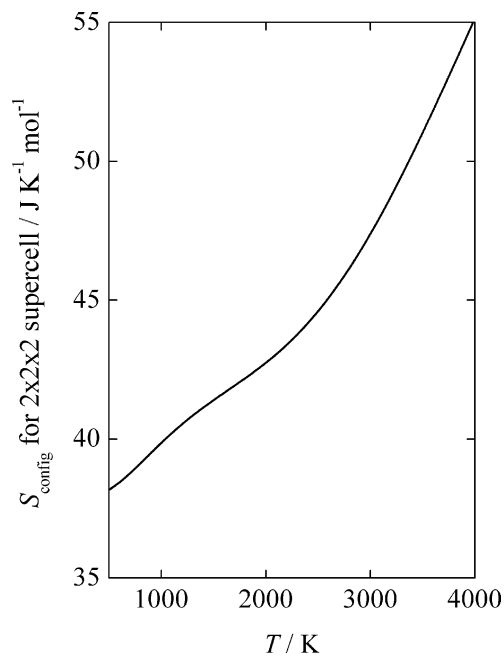
Fig. 7. Configurational entropy as a function of temperature.

the configurational entropy is not negligible even below 2000 K (see Fig. 7). Above 2000 K, the number of square pyramids increases giving a smaller number of tetrahedra and octahedra, see Fig. 6. Only at the highest temperatures is a small number of polyhedra with three coordinate indium observed. The 3-coordinate In-atoms are present together with 5-coordinate In-atoms in CNCs closely related to (00404) CNCs and these can equally well be viewed as distorted (00404)s.

The population of intermediate-energy CNCs also affects the calculated configurational entropy which increases faster above 2000 K. It is tempting to suggest a correlation between the observation of an apparent intermediate structure by diffraction [4,5] and NMR-experiments [5], and the change in slope of the entropy-temperature curve in Fig. 7. This change in slope then relates to the formation of the cubic structure. Our results are in line with the entropy of the disordered phase being considerably lower than the ideal value [33,34] since only a small fraction of the possible CNCs are thermally accessible at these temperatures and thus, due to the presence of only a small number of structural polyhedral entities, the arrangement of the oxygen vacancies remains far from random.

Our results call into question the very form in which the so-called "ideal" configurational entropy is introduced into empirical models. This generally starts from a simple evaluation of the number of ways a given number of vacancies can be distributed at random over a number of lattice sites, ignoring any complications associated with relaxation of the structure, the form of the potential energy hypersurface and the associated

preference for particular structural polyhedra. For the $2 \times 2 \times 2$ cell there are 10626 permutations of the 20 oxygen atoms over 24 oxygen lattice sites. Nevertheless the total number of relaxed configurations, after structure optimization, is considerably higher ($\approx 21{,}500$). After relaxation the symmetry of a CNC, and thus its degeneracy, may be very different from that of the idealized configuration used as a starting point. It is the degeneracy of the relaxed configuration which should be used in all thermodynamic averaging. The number of possible sites available for the oxygen atoms is large but strong structural correlations due to the preference for particular structural polyhedra mean that these will be far from randomly occupied. Thus, presently used defect models that describe the structures and thermodynamics of this and related materials in terms of random distributions of oxygen atoms and oxygen vacancies over the available oxygen sites in an idealized lattice are highly questionable from a fundamental point of view, even if they often serve as useful empirical models (see, e.g., Ref. [35] which uses such an approach to analyze the redox energetics of perovskite-type oxides).

The relative energies of the different local structural environments have important implications for the ionic conductivity of the material. The conventional vacancy jump mechanism would allow different types of local short-range order that we here show are of high energy and thus make a negligible contribution. The ionic movement is highly restricted by the local symmetry as seen e.g. by the high energy of the square-planar entity compared to a tetrahedral local structure. The occupancy of the O(1), O(2) and O(3) sites shown in Fig. 8 completes the picture. O(1) and O(2) are fully populated to 1500 K after which the population of O(2) decreases significantly. O(1) is fully populated to significantly higher temperatures which supports the two-dimensional disorder and conductivity at intermediate temperatures reported previously [5]. The very nature of the low-energy structural configurations has even more extensive fundamental implications for the ionic conductivity. Transition paths connecting different low-energy CNCs characterized using the Nudge-elastic-band method strongly indicate that collective ion movements are important in fast oxide-ion conductors such as $Ba_2In_2O_5$ [9]. This aspect will be discussed in detail in a forthcoming contribution concentrating on saddle points on the energy hypersurface and on the nature of different possible transition paths.

4. Summary

In this paper the structural features of $Ba_2In_2O_5$ at high temperatures have been investigated through a thorough study of the full energy hypersurface of a
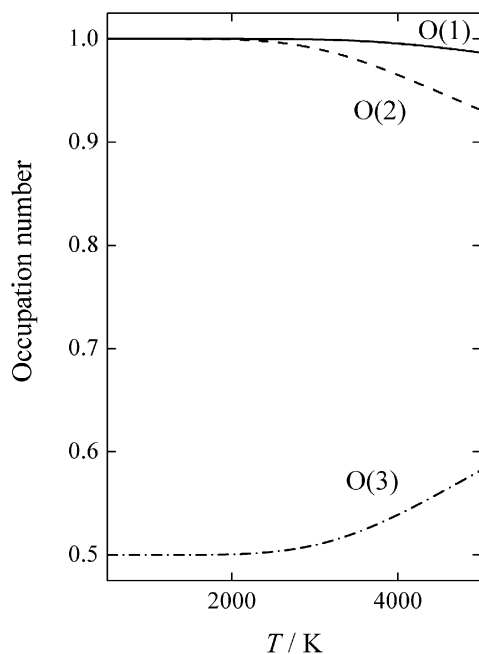
Fig. 8. Occupancy of the three oxygen sites as a function of temperature.

36-atoms supercell. We interpret the average structure observed experimentally at any temperature as a time and spatial average of the different local environments (corresponding to separate local minima on the potential energy surface) which are energetically accessible at that temperature. These environments are regarded as representing snapshots of small regions of the disordered material and thus to show local structural environments and structural correlations. The distribution of oxygen vacancies is far from random and relatively few configurations, associated with different arrangements of tetrahedral InO_4, square pyramidal InO_5 and octahedral InO_6 entities, are thermally accessible at most temperatures. The brownmillerite-type ground state structure is reproduced by the calculations. In addition, many of the lower energy minima resemble this ground state structure in that they consist of alternating layers of InO_4-tetrahedra and InO_6-octahedra. These configurations differ in the stacking sequences of the tetrahedral layers, and in the type of connectivity within the tetrahedral layers. Other configurations i.e. the structures adopted by $Sr_2Mn_2O_5$ and $La_2Ni_2O_5$ are also discussed in some detail. The energies of the configurations are in general largely influenced by the positions of the large Ba ions and thus by the Ba–O interactions. These interactions are easily characterized using bond valence sums which are shown to correlate well with the energy for selected groups of related CNC's.

The results for the chosen supercell are furthermore used for considering stacking-sequences and connectiv-ity-patterns present only in larger brownmillerite-related supercells. The existence of a range of different CNCs close in energy rationalises the frequent observation of incompletely ordered structures even at room-temperature. At low temperatures the energy barriers from one minimum to another are thermally inaccessible. Complete long-range order is thus not easily achieved and frozen-in disorder results. It is interesting in this connection that the freezing of rapid oxygen ordering recently has been reported to give rise to glass-like transitions in perovskite-related oxides [36] as well as in $ZrWMoO_8$ [37].

Although the (00404)-CNCs dominate at low temperatures disorder is not negligible. The range of different (00404)-configurations close in energy gives rise to significant disorder and imply that the configurational entropy is not negligible even below 2000 K. Our results are in line with the entropy of the disordered phase being considerably lower than the ideal value. The number of possible sites available for the oxygen atoms is large but strong structural correlations due to the preference for particular structural polyhedra imply that these will be far from randomly occupied.

The energetic preference for certain structural entities also has implications for ionic transport due to restraints imposed by local symmetry. The conventional vacancy jump mechanism requires different types of local short-range order that we have shown here are of high energy and thus make a negligible contribution; thus the ionic movement is highly restricted by the local symmetry. O(1) and O(2) are fully populated to 1500 K after which the population of O(2) decreases significantly. O(1) is fully populated to significantly higher temperatures which supports the two-dimensional disorder and conductivity at intermediate temperatures reported previously. The very nature of the low-energy structural configurations has even more extensive fundamental implications for the ionic conductivity. Transition paths connecting different low-energy CNCs characterized using the Nudge-elastic-band method strongly indicates that collective ion movements are important in fast oxide-ion conductors such as $Ba_2In_2O_5$.

References

[1] D.H. Gregory, M.T. Weller, J. Solid State Chem. 107 (1993) 134–148.

[2] J.B. Goodenough, J.E. Ruiz-Diaz, Y.S. Chen, Solid State Ion. 44 (1990) 21–31.

[3] P. Berastegui, S. Hull, F.J. Garcia-Garcia, S.-G. Eriksson, J. Solid State Chem. 164 (2002) 119–130.

[4] S.A. Speakman, J.W. Richardson, B.J. Mitchell, S.T. Misture, Solid State Ion. 149 (2002) 247–259.

[5] S.B. Adler, J.A. Reimer, J. Baltisberger, U. Werner, J. Am. Chem. Soc. 116 (1994) 675–681.

[6] A.M. Abakumov, A.M. Alekseeva, M.G. Rozova, E.V. Antipov, O.I. Lebedev, G. Van Tendeloo, J. Solid State Chem. 174 (2003) 319–328.

[7] S. Adler, S. Russek, J. Reimer, M. Fendorf, A. Stacy, Q. Huang, A. Santoro, J. Lynn, J. Baltisberger, U. Werner, Solid State Ion. 68 (1994) 193–211.

[8] M. Kanzaki, A. Yamaji, Mater. Sci. Eng. B 41 (1996) 46–49.

[9] C.E. Mohn, N.L. Allan, C.L. Freeman, P. Ravindran, S. Stølen, Phys. Chem. Chem. Phys. 6 (2004) 3052–3055.

[10] G. Kresse, J. Hafner, Phys. Rev. B 47 (1993) 558–561.

[11] G. Kresse, J. Joubert, Phys. Rev. B 59 (1999) 1758–1775.

[12] N.L. Allan, G.D. Barrera, R.M. Fracchia, M.Yu. Lavrentiev, M.B. Taylor, I.T. Todorov, J.A. Purton, Phys. Rev. B 63 (2001) 094203.

[13] E. Bakken, N.L. Allan, T.H.K. Barron, C.E. Mohn, I.T. Todorov, S. Stølen, Phys. Chem. Chem. Phys. 5 (2003) 2237–2243.

[14] I.T. Todorov, N.L. Allan, M. Yu. Lavrentiev, C.L. Freeman, C.E. Mohn, J.A. Purton, J. Phys.: Condens. Matter 16 (2004) S2751–S2770.

[15] J.B. Wiley, M. Sabat, S.-J. Hwu, K.R. Poeppelmeier, A. Reller, T. Williams, J. Solid State Chem. 87 (1990) 250–260.

[16] I.D. Brown, R.D. Shannon, Acta Crystallogr. A 29 (1973) 266–282.

[17] S. Lambert, H. Leligny, D. Grebille, D. Pelloquin, B. Raveau, Chem. Mater. 14 (2002) 1818–1826.

[18] S.Ya. Istomin, J. Grins, G. Svensson, O.A. Drozhzhin, V.L. Kozhevnikov, E.V. Antipov, J.P. Attfield, Chem. Mater. 15 (2003) 4012–4020.

[19] L.J. Gillie, H.M. Palmer, A.J. Wright, J. Hadermann, C. Van Tendeloo, C. Greaves, J. Phys. Chem. Solids 65 (2004) 87–93.

[20] F. Liebau, Structural Chemistry of Silicates: Structure, Bonding and Classification, Springer, Berlin, Heidelberg, 1985, pp. 78–82.

[21] V. Caignaert, N. Nguyen, M. Hervieu, B. Raveau, Mater. Res. Bull. 20 (1985) 479–484.

[22] K.R. Poeppelmeier, M.E. Leonowicz, J.M. Longo, J. Solid State Chem. 44 (1982) 89–98.

[23] P. Adler, U. Schwarz, K. Syassen, A.P. Milner, M.P. Pasternak, M. Hanfland, J. Solid State Chem. 155 (2000) 381–388.

[24] L. Er-Rakho, C. Michel, P. Lacorre, B. Raveau, J. Solid State Chem. 73 (1988) 531–535.

[25] J.P. Chapman, J.A. Attfield, M. Molgg, C.M. Friend, T.P. Bealers, Angew. Chem. Int. Ed. Engl. 35 (1996) 2482–2484.

[26] D. Akahoshi, Y. Ueda, J. Solid State Chem. 156 (2001) 355–363.

[27] K. Vidyasagar, J. Gopalakrishnan, C.N.R. Rao, Inorg. Chem. 3 (1984) 1206–1210.

[28] M.T. Anderson, J.T. Vaughey, K.R. Poeppelmeier, Chem. Mater. 5 (1993) 151–165.

[29] K. Vidyasagar, A. Reller, J. Gopalakrishnan, C.N.R. Rao, Chem. Commun. (1985) 7–8.

[30] R. Grenouel, C. Michel, N. Nguyen, M. Hervieu, B. Raveau, J. Solid State Chem. 115 (1995) 469–475.

[31] M.L. Ruiz-Gonzalez, C. Prieto, J. Alonso, J. Ramirez-Castellanos, J.M. Gonzalez-Calbet, Chem. Mater. 14 (2002) 2055–2062.

[32] M.L. Ruiz-Gonzalez, J. Ramirez-Castellanos, J.M. Gonzalez-Calbet, J. Solid State Chem. 155 (2000) 372–380.

[33] T.R.S. Prasanna, A. Navrotsky, J. Mater. Res. 8 (1993) 1484–1486.

[34] T. Hashimoto, Y. Ueda, M. Yoshinaga, K. Komazaki, K. Asaoka, S.R. Wang, J. Electrochem. Soc. 149 (2002) A1381–A1384.

[35] E. Bakken, T. Norby, S. Stølen, J. Mater. Chem. 12 (2002) 317–323.

[36] A.I. Rykov, K. Nomura, T. Matsui, M. Seto, Physica B 350 (2004) 287–304.

[37] S. Allen, J.S.O. Evans, J. Mater. Chem. 14 (2004) 151–156.